NMR Study of Optically Active Monosubstituted Cryptophanes and Their Interaction with Xenon

J. Gaspard Huber,[†] Lionel Dubois,[†] Hervé Desvaux,[†] Jean-Pierre Dutasta,[‡] Thierry Brotin,[‡] and Patrick Berthault*[,†]

DSM/DRECAM, Service de Chimie Moléculaire, URA CEA/CNRS 331 Claude Fréjacques, CEA/Saclay, 91191 Gif sur Yvette, France, and Stéréochimie et Interactions Moléculaires, UMR CNRS 5532, Ecole Normale Supérieure de Lyon, 46 Allée d'Italie, 69364 Lyon 07, France

Received: June 28, 2004; In Final Form: August 20, 2004

The study of the interaction between xenon and two cryptophane derivatives in organic solution has been carried out through ^{1}H and ^{129}Xe NMR. The cage molecules constituted by the grafting of (−)-camphanic acid are diastereomers through the orientation of the ethylenedioxy linkers joining the cyclotriveratrylene moieties. The availability of laser-polarized xenon has allowed us not only to perform ^{129}Xe spectra at a low concentration of dissolved gas but also to perform magnetization-transfer experiments from xenon to protons, confirming the inclusion of noble gas atoms into the cryptophane cavities. Binding constants of xenon in diastereomers were compared, as well as xenon exchange rates in the cryptophane cavities. A detailed structural and dynamic study performed with help of off-resonance ROESY experiments gave precious local information. The cryptophane derivative with the highest affinity for xenon seems to be the most able to distort its cavity to fit the xenon atom. In the complex, the cavity is elongated, and the noble gas atom can find different locations. This seems to indicate that the entropy contribution is also important in explaining the difference in affinity of xenon between these cage molecules. These results clearly show that in the design of new cage molecules for biosensing, the separation of cryptophane diastereomers is important because their affinity and their properties vis-à-vis xenon can be strongly different.

Introduction

Cryptophanes belong to a fascinating class of molecules because these aromatic hosts are able to encapsulate apolar neutral guests strongly; therefore, they constitute powerful tools for understanding the bases of molecular recognition. For example, the binding constant with xenon has been measured to be as high as ca. 3900 M^{-1} at 278 K for cryptophane-A in 1,1,2,2-tetrachloroethane.[1] Moreover, these cagelike host molecules are promised to find several concrete applications, from gas sensors[2] to biosensors.[3] In this last project, the high sensitivity of ^{129}Xe combined with its wide chemical shift range is used to perform multiplexed "intelligent" MRI. The ability to enhance the NMR signal of the noble gas by several orders of magnitude thanks to optical pumping, combined with the capacity of cryptophane derivatives to transport it to specific biological targets, opens the way toward very interesting molecular imaging approaches. The functionalization of the cryptophanes, required in such an approach, transforms the enantiomers into diastereomers as soon as an asymmetric carbon is attached to the cryptophane moiety. It can, however, be important to the design of the host molecule to avoid the presence of diastereomers because each of them may produce a xenon NMR signal at a different chemical shift, uselessly spreading the information and lowering the signal-to-noise ratio of the images. Because the diastereomers can be isolated by HPLC or crystallization,[4] a fine characterization of the structure and dynamics of both diastereomers seems important not only to help choose the best candidate but also to give insight into molecular host−guest recognition.

By way of the design of cryptophane derivatives that may be used in biosensing, we have decided to characterize two optically active monosubstituted cryptophanes, the two diastereomers of the reaction product of the anti (−)-cryptophanol A and (−)-camphanic acid chloride, **1a**, and anti (+)-cryptophanol A and (−)-camphanic acid chloride, **1b**. These two compounds (Figure 1) have been previously identified by circular dichroism, and the diastereomeric purity (de = 98−100%) has also been assessed by NMR.[4] The thermodynamic and kinetic parameters of the xenon binding are discussed through competition experiments with cryptophane-A using laser-polarized xenon. Moreover, a series of off-resonance ROESY experiments are used to derive the solution structures of **1a** and **1b** in deuterated tetrachloroethane in the presence of xenon pressure high enough to consider that all of the cryptophane cages are filled. These experiments also provide data about internal dynamics, which are used in a comparative manner between the two hosts. The variation of ^{1}H chemical shifts between both diastereomers is then discussed with regard to the expected influence of aromatic rings and serves to confirm the previously determined preferential solution structures.

Results and Discussion

Determination and Comparison of Thermodynamic and Kinetic Constants. The ^{129}Xe NMR spectra of a mixture of cryptophane-A, **1a** and **1b**, in deuterated tetrachloroethane at 283 K under two xenon pressures are presented in Figure 2.

* To whom correspondence should be addressed. E-mail: pberthault@cea.fr. Fax: +33 1 69 08 98 06. Tel: +33 1 69 08 42 45.
[†] DSM/DRECAM.
[‡] Ecole Normale Supérieure de Lyon.

10.1021/jp0472055 CCC: $27.50
Published on Web 10/13/2004

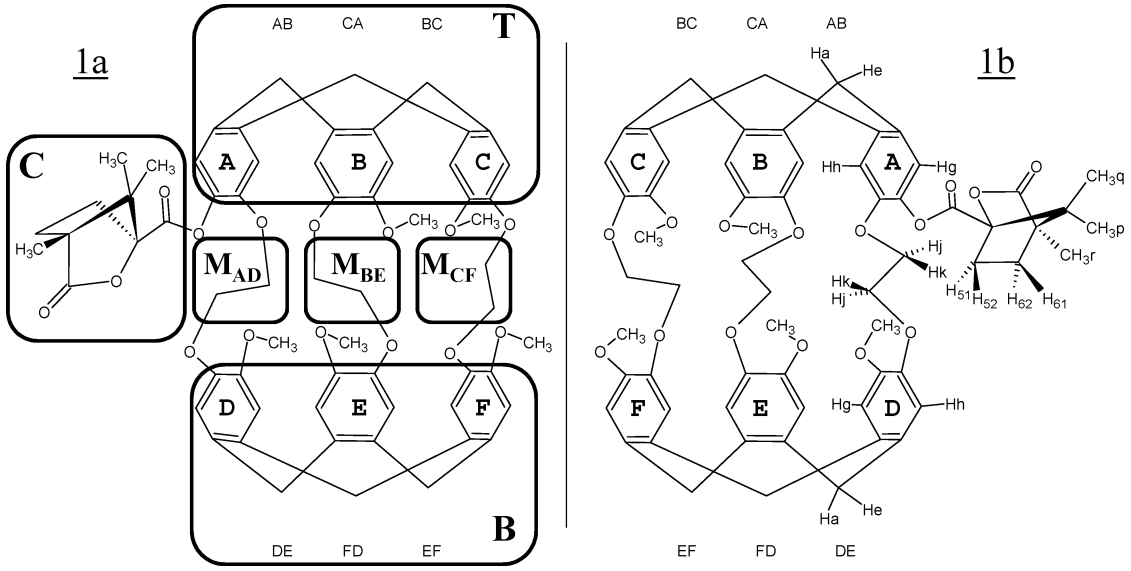

Figure 1. Nomenclature of compounds **1a** and **1b** adopted in the present article, following that used by Bartik et al. for cryptophane-A.[1] The nomenclature for protons and methyl groups is explained for **1b** and is defined in a similar way for **1a**. T, B, M_{AD}, M_{BE}, M_{CF}, and C classes used for the discussion of internal dynamics are explained for **1a** and defined similarly for **1b**.

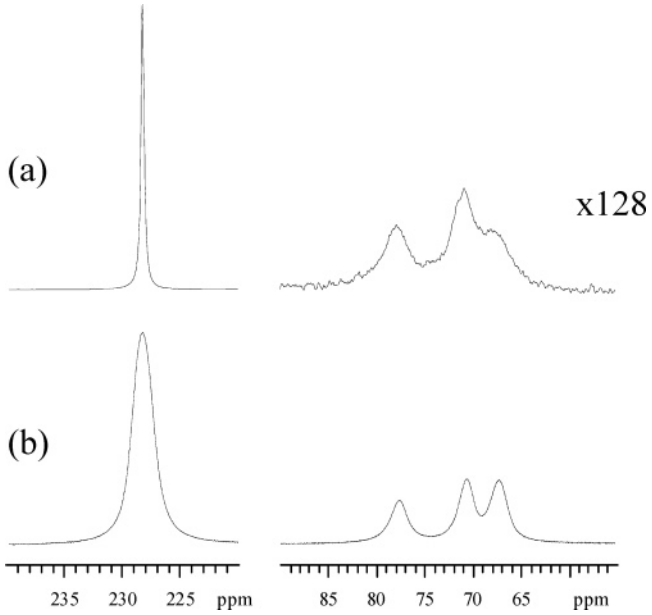

Figure 2. Laser-polarized ^{129}Xe NMR spectrum of a mixture of cryptophane-A/**1a**/**1b** at 283 K under ^{129}Xe pressures of (a) 99 kPa and (b) 5.3 kPa. The concentrations are 2.80, 1.34, and 1.46 mM, respectively. The xenon pressure above the solution was estimated after having expanded the gas in a volume equipped with a pressure gauge. The lower signal-to-noise ratio in spectrum a is due to a lower polarization of xenon when the experiment was performed. From downfield to upfield, signals are assigned to xenon free in solution and xenon bound to **1a**, **1b**, and cryptophane-A, respectively.

The availability of laser-polarized xenon with nuclear magnetization enhanced by several orders of magnitude gives access to experiments with low (5.3 kPa) and medium (99 kPa) gas pressures. The spectra exhibit four signals in slow exchange on the xenon chemical shift time scale. The downfield signal is assigned to xenon that is free in solution, as previously shown for cryptophane-A in deuterated tetrachloroethane.[5] The assignment of the three other signals is obtained by repeating the experiments first after adding of a small amount of cryptophane-A to the solution and, in a second step, after adding a small amount of **1a**. The three signals are assigned to xenon bound to **1a**, **1b**, and cryptophane-A, respectively, from low field to high field.

Xenon chemical shift variations up to 1.2 ppm have previously been observed according to deuterium−proton isotopic substitution in cryptophane-A.[6] Chemical shift variations of ca. 1 ppm have also been reported in monosubstituted cryptophane-A depending on the substituent type.[3] When this substituent binds a given protein, an additional chemical shift variation of less than 2 ppm is observed, representing the basis of biosensing.[3,7] In the present study, a chemical shift difference of ca. 7 ppm is observed for the signals of xenon bound to **1a** and **1b**. Xenon chemical shifts even differ by more than 10 ppm between **1a** and cryptophane-A. The amplitude of these variations should reveal strong structural modifications between these two diastereomers.

The volume of the cavity is a dominant parameter for the interpretation of the large xenon chemical shift variations between cryptophanes.[8] For example, the chemical shift value of xenon bound to cryptophanes increases when following the series cryptophane-333 (i.e., cryptophane-E)/cryptophane-233/cryptophane-223/cryptophane-222 (i.e., cryptophane-A), where each number indicates the number *n* of carbon atoms in the $O-(CH_2)_n-O$ linkers.[9] In this series, the cage volume is decreasing. Difference in the cage volumes of **1a**, **1b**, and cryptophane-A could thus explain the xenon chemical shift variation. Another reason for this variation can be the shielding effect of nearby atoms or atom groups. In the case of **1a** and **1b**, the orientation of the camphanate moiety can lead to a different influence of the carbonyl groups on the chemical shift of bound xenon.

^{1}H NMR spectra of the **1a**/**1b** mixture (data not shown) at 5.3 and 99 kPa of xenon essentially exhibit signals assigned to the cages binding a xenon atom. Integration of the H51 signals (from the camphanic moiety, vide infra), highly resolved for both molecules, gives **1a**/**1b** relative proportions of 47.9:52.1 ± 0.9. Because this ratio is independent of the experimental xenon pressure, other forms, for example, where the cage does not contain a xenon atom, are either in negligible concentration or in fast exchange with the bound form. Peak areas on the ^{129}Xe NMR spectra indicate the relative concentration of each cage−xenon complex and of xenon free in solution. Under a

TABLE 1: Proton Chemical Shifts of 1a and 1b in d_2-1,1,2,2-Tetrachloroethane at 281 K under a Xenon Gas Pressure of ca. 170 kPa[a]

	1a							1b					
	A	B	C	D	E	F		A	B	C	D	E	F
Hg	6.914	6.651	6.619	6.648	6.85	6.598	Hg	6.810	6.619	6.613	6.636	6.742	6.576
Hh	6.737	6.745	6.645	6.761	6.628	6.614	Hh	6.669	6.624	6.627	6.716	6.572	6.610
OCH_3		3.864	3.845	3.861	3.997	3.833	OCH_3		3.846	3.847	3.844	3.906	3.828
Hj	3.859	3.946	4.053	3.858	4.059	3.946	Hj/Hk	?	?	4.050	3.835	3.953	4.055
Hk	4.415	4.445	4.316	4.547	4.331	4.356	Hk/Hj	4.401	4.456	4.343	4.589	4.559	4.341
	AB	BC	CA	DE	EF	FD		AB	BC	CA	DE	EF	FD
Ha	4.494	4.583	4.696	4.420	4.622	4.586	Ha	4.500	4.549	4.663	4.409	4.596	4.544
He	3.419	3.382	3.465	3.441	3.378	3.365	He	3.376	3.375	3.457	3.339	3.369	3.355
H52	H51	H61	H62	p	q	r	H52	H51	H61	H62	p	q	r
2.189	2.640	1.809	2.063	1.198	1.386	1.239	2.298	2.882	1.826	2.126	1.449	1.147	1.203

[a] Hj (respectively Hk) corresponds to the pro-R (respectively pro-S) proton. Hj and Hk protons are not stereospecifically assigned for **1b**.

xenon pressure of 5.3 kPa, **1a**-Xe and **1b**-Xe are in the proportion 43.7:56.3 ± 1.2. This attests to the fact that **1b** binds xenon more favorably than **1a** does.

From the spectrum acquired at 5.3 kPa, a lower limit of the binding constants of **1a** and **1b** with xenon can be computed using the value of 3400−4400 M^{-1} measured for xenon in cryptophane-A at 278 K.[1] First, the cryptophane-A/xenon binding constant at 283 K has to be estimated. The entropy and enthalpy may be evaluated from experimental values for the cryptophane-A/chloroform complex. Because of the large volume of chloroform (72 Å^3), the ethylenedioxy groups of cryptophane-A adopt a conformation that maximizes the volume of the cage (95 Å^3). The rigidity of the complex explains the large destabilizing entropy of −67 J·mol^{-1}K^{-1}.[10] The volume of xenon is smaller, 42 Å^3; therefore, its entropy of complex formation with cryptophane-A is higher than −67 J·mol^{-1}K^{-1}. Assuming this lower estimate of entropy and a possible error of 10% in cryptophane-A and **1a**−**1b** racemic mixture concentrations and taking the recently measured xenon−tetrachloroethane solubility to be 1.00 μM·Pa^{-1} [11]), lower limits of the binding constants for xenon have been estimated from the fitted area of the three upfield peaks of Figure 2b to be 2000 and 3200 M^{-1} for **1a** and **1b**, respectively. This implies that at 170 kPa and for the solute concentrations used in the structural and dynamics studies (see below), more than 99.7% of the cage molecules are occupied by a xenon atom.

Besides thermodynamics considerations, kinetics data may be extracted from NMR spectra. The slow exchange conditions enable the estimation of xenon dissociation rate values inside the cavities from signal line width measurements. We have verified that line broadening is due to neither magnetic field inhomogeneity nor temperature dispersion.

At 5.3 kPa (Figure 2b), the line widths for xenon bound to the cage molecules are very similar; therefore, considering the weak contribution of dipolar interactions to transverse relaxation, dissociation rate values are estimated to be 0.9, 0.7, and 0.8 kHz for **1a**, **1b,** and cryptophane-A, respectively. At 99 kPa, a significant increase is noted for cryptophane-A (1.8 kHz) but is less pronounced for **1a** (1.3 kHz) and **1b** (1.2 kHz). Conversely, the signal from xenon free in solution becomes sharper when passing from 5.3 to 99 kPa.

It was shown that there is no direct exchange between cages in the case of cryptophane-A.[6] Assuming that this may be extended to substituted cryptophane-A molecules such as **1a** and **1b**, we can qualitatively explain our experimental results through a simple xenon−cage complex model and the following associated equations for each cage molecule C:

$$\mathrm{Xe} + \mathrm{C} \underset{k_{-1}}{\overset{k_{+1}}{\rightleftharpoons}} \mathrm{Xe{-}C}$$

$$K = \frac{[\mathrm{XeC}]}{[\mathrm{Xe}][\mathrm{C}]} = \frac{k_{+1}}{k_{-1}}$$

$$k_{+1}[\mathrm{C}] = \frac{1}{\tau_{\mathrm{Xe}}} = \frac{k_{-1}[\mathrm{XeC}]}{[\mathrm{Xe}]}$$

where k_{+1} and k_{-1} are the complexation and dissociation rates of the xenon−cage complex, respectively, K represents the binding constant, and [C], [XeC], and [Xe] are the concentrations of noncomplexed cages, complexed cages, and xenon free in solution, respectively. k_{+1}[C] thus represents the complexation rate of xenon to any cage molecule (i.e., the reverse of the residence time of xenon free in solution τ_{Xe}). At low gas pressure (5.3 kPa compared to 99 kPa), fewer xenon atoms are dissolved, and binding equilibria are displaced toward the nonbound states. From the xenon point of view, complexation rate k_{+1}[C] is higher: the line associated to xenon free in solution is broader. From the cage point of view, the collisions giving rise to the exchange are scarcer, and therefore exchange rates k_{+1} and k_{-1} are smaller. Thus, the lines associated with xenon bound in cryptophanes are narrower.

Subtle differences between the three cages present in this experiment may thus be outlined: it appears that xenon bound to **1b** is less subjected to exchange than xenon bound to **1a** and that cryptophane-A is the most exposed. These results imply not only that **1b** binds xenon with a higher affinity than **1a** but also that the dissociation rate for the former complex is lower than for the latter (and for the complex with cryptophane-A). Because the only structural difference between these cage molecules lies in the camphanate grafting, one hypothesis is that the camphanate group could influence xenon's access to the cavity.

To correlate these results to molecular properties, it is appropriate to describe the structure and the dynamics of these compounds in solution, the first step being the assignment of the proton signals.

NMR: ^{1}H Assignment and NOE Data. The cryptophane diastereomers have been studied under a xenon pressure for which they are almost always filled with a noble gas atom

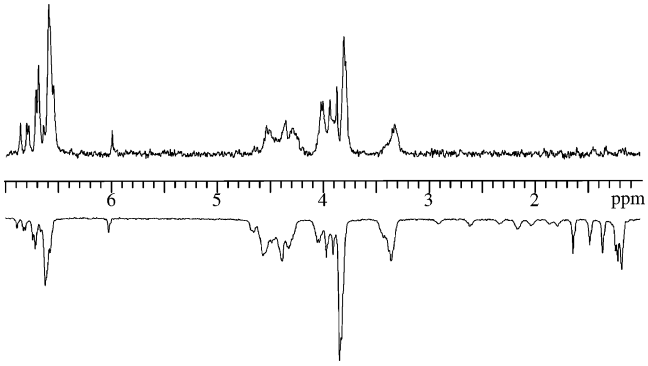

Figure 3. SPINOE (top) and ^{1}H NMR spectrum (bottom) of a racemic mixture of **1a** and **1b** at 288 K, 11.7 T. In this SPINOE subspectrum performed with a mixing time of 500 ms, only protons of the cryptophane moiety are detected.

(xenon pressure 170 kPa). Thus, proton NMR observables, particularly chemical shifts, account for the bound form.

The proton assignment of **1a** and **1b** is given in Table 1 using the nomenclature of Figure 1. All protons except two belonging to the ethylenedioxy linkers of **1b** are assigned. The stereospecific assignment of the Hj and Hk protons for **1a** is made possible using geometric considerations from a first set of structures obtained via NOE data. It is interesting that the complete set of Hj resonances is shifted upfield with respect to the Hk set. This is in accordance with ring current effects from the aromatic cycles on these protons predicted through a simulation, as discussed later. For **1b**, the stereospecific assignment of Hj and Hk protons is less clear because the lower number of NOE data available and the lack of assignment of two protons of the linkers preclude the safe use of molecular modeling considerations. Proton signal coalescence, observable, for instance, in HSQC spectra, may explain these uncertainties. Therefore, no stereospecific assignment of the linkers has been made for **1b**.

Similarly, the stereospecific assignment of the methylene bridges (protons Ha and He) performed using considerations of NOE data (see Material and Methods) has been confirmed by a simple simulation of ring current effects on these protons.

The solution structures are determined using proton−proton distance restraints extracted from off-resonance ROESY experiments performed at various mixing times and various angles between the spin-lock axis and the static field axis. This method enables the derivation of proton−proton distances without the use of an internal distance reference and the estimation of local correlation times.[12]

The number of unambiguous experimental restraints is higher for **1a** (58 proton−proton distances and correlation times) than for **1b** (47 restraints). This is explained by the higher chemical shift dispersion for the former compound. Six camphanate−cage NOE data are observed in **1a**, and nine are observed in **1b**.

NMR: Xenon−Proton Interaction. As experimental proof that the xenon atom is really included in the cryptophane cavity and that the camphanate moiety neither forbids this inclusion nor binds xenon with a significant affinity, a SPINOE[13−15] spectrum was recorded for a diastereomeric mixture of **1a** and **1b** (Figure 3). The ^{1}H signals present on the subspectra belong only to the cryptophane moiety, confirming this idea. The expected in-phase character of the SPINOE signals, arising from dipolar interaction between xenon and protons, is observed and depends on the sign of the noble gas polarization. The relative SPINOE intensities of aromatic and He protons clearly confirm

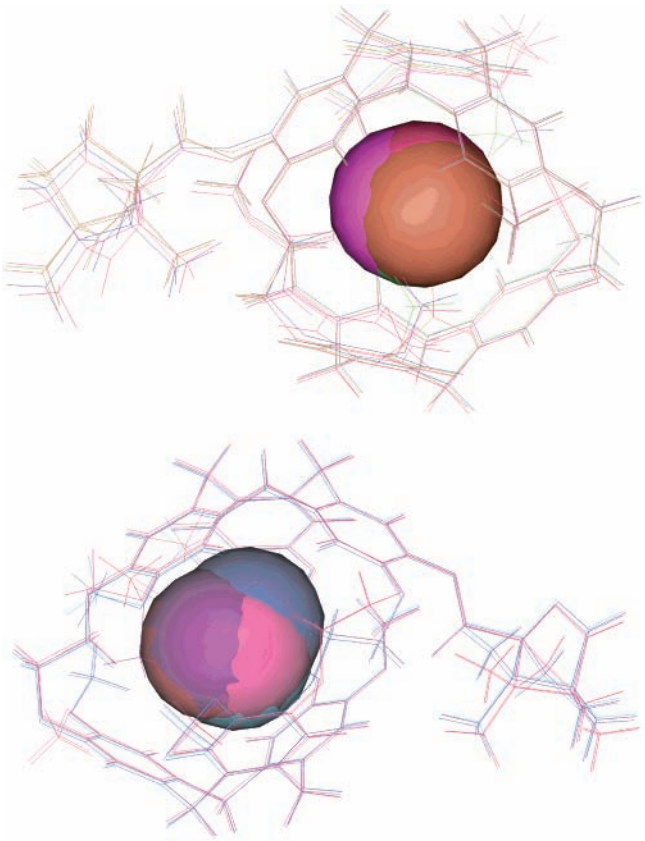

Figure 4. Superimposition of five low-energy structures of **1a** (top) and **1b** (bottom). The xenon atoms in the cavities are represented by their van der Waals spheres. See the text for further explanations.

that xenon is located inside the cavity. This is consistent with magnetization transfer from laser-polarized xenon to protons on cryptophane-A[5] and cryptophane-233, where two ethylenedioxy linkers of cryptophane-A are replaced by propylenedioxy linkers.[16]

Molecular Modeling: Structure Comparison. For each diastereomer, the proton−proton distance restraint set is used in a simulated annealing procedure repeated 100 times with random initial atomic velocities, leading to 100 structures. The simulated annealing procedure under NOE restraints is performed with and without an explicit xenon atom of diameter 4.46 Å placed at the center of the cavity. The pairwise rms deviation of the coordinates of the heavy atoms of the cryptophane moiety does not decrease significantly when an explicit xenon atom is placed at the center of the cavity during simulated annealing, indicating no tight fitting of xenon inside the cavity, which would limit the degrees of freedom for the relative motions of both cyclotriveratrylene groups.

With the same criteria based on the total energy value and the absence of NOE violations being applied to **1a** and **1b**, 53 structures are finally accepted for **1a** and 60 are accepted for **1b**. Back calculation of the proton−proton distances performed on the average structures is fully consistent with the experimental off-resonance ROESY spectra, the only lack of experimental restraints for protons in close proximity being due to spectral overlap. For **1a**, the pairwise rms deviation is 0.406 Å when considering the "backbone" atoms (i.e., the carbon atoms of the cryptophane part, except those of the ethylenedioxy linkers and the methoxy groups). For **1b**, the pairwise rms deviation is 0.404 Å.

Five structures among the accepted ones for **1a** and **1b** are superimposed in Figure 4. The main orientations of the

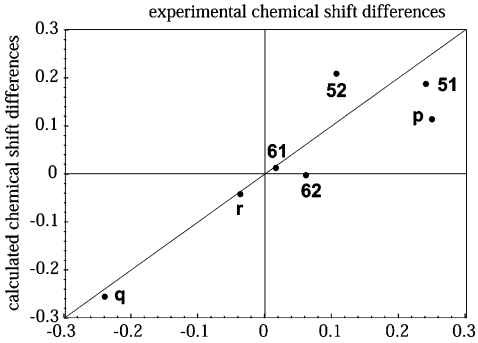

Figure 5. Calculated vs experimental **1b** − **1a** chemical shift differences due to ring current effects on camphanate protons. (See the text for the equation.)

camphanate part with respect to the cryptophane moiety are different. The carbonyl group attached to the cryptophane points toward the cage in **1b**, whereas it is exposed to the solvent in **1a**. In both molecules, methyl q is the closest camphanate element relative to the cage. However, this group is in close proximity to D-Hk proton in **1a**, whereas it is close to A-Hj proton in **1b**.

It is clear in Figure 4 that the cavity of **1b** is more elongated than that of **1a**. This is related to nonambiguous NOE cross peaks between protons belonging to two different linkers in **1b**, whereas no equivalent NOE appears for **1a**.

Also, xenon is less localized inside the cavity of **1b** than in **1a** (root-mean-square deviation of xenon from its average location: 0.43 Å in **1a**, 0.73 Å in **1b**). This higher disorder observed for the complex with **1b** than with **1a** may involve a higher entropy contribution and can be related to our experimental result of a higher binding constant with xenon for **1b** than for **1a**.

The structures of lowest energy for **1a** and **1b** exhibit two ethylenedioxy spacers in the anti conformation (considering the oxygen atoms), the last spacer being more fluctuant, spending the majority of its time in the gauche conformation. This observation is in accordance with the conclusions of Bartik et al.[1] from their measurement of $^1H-^1H$ scalar couplings and with the results of Lühmer et al.[5] in their analysis of SPINOE for xenon in cryptophane-A. The dispersion around these canonical dihedral angle values is, however, more pronounced for **1b** than for **1a**. The root-mean-square deviation of the ethylenedioxy linker carbons from the average structure is 0.24 Å for **1a** and 0.43 Å for **1b**.

The ring current effects induced by the cyclotriveratrylene moieties on the camphanate protons have been predicted via a simplistic dipolar law of the form

$$\Delta\delta_i = f\sum_j (1 - 3\cos^2\theta_{ij}) r_{ij}^{-3}$$

where r_{ij} is the distance between proton i under consideration and the center of the aromatic ring j, θ_{ij} is the angle between the vector r_{ij} and the normal to aromatic plane j, and f is a proportionality constant. For a given proton, the difference in experienced ring current effects in **1a** and **1b** can help in positioning the camphanate moiety relative to the cryptophane cage. Good correlation between the predicted chemical shift differences and the experimental data is obtained, with a correlation factor of 0.82, confirming the quality of the structures (Figure 5).

Dynamics on the Nanosecond Time Scale. From the set of off-resonance ROESY experiments performed at different angles between the spin-lock axis and the static field axis, dipolar correlation times (τ_c) per pair of protons[12] in **1a** and **1b** in the presence of xenon have been extracted. These data can give access to local dynamics. It is hardly possible to interpret individually them because of their relative imprecision. (However, this method has been shown in ref 12a to be more precise and accurate for solution structure determination than the conventional internal reference distance method.) Neither the cyclotriveratrylene subunits (except for methoxy groups) nor the camphanate moieties have an allowed degree of internal free rotation. Therefore, they should confer the same dynamic behavior to the protons they contain, and a qualitative interpretation of these data can be performed by grouping proton−proton correlation times according to the part of the molecule to which they belong. Hg and Hh protons of cycles A, B, and C and Ha and He of the methylene bridges linking these cycles are considered to belong to the top cryptophane bowl, when drawing the molecules as in Figure 1, and form the first class named T (top). (See Figure 1 for the definition of classes in molecule **1a**, similar classes being defined for **1b**.) Similarly, D, E, F, DE, EF, and FD correspond to the bottom cryptophane bowl, which therefore belongs to class B (bottom). The three ethylenedioxy linkers are expected to be subjected to a different local mobility. Corresponding protons are grouped into classes M_{AD}, M_{BE}, and M_{CF} for AD, BE, and CF linkers, respectively. Finally, the camphanate moiety is referred to as class C. The number of extracted τ_c values in **1b** is smaller than that in **1a** because of a higher fraction of superimposed cross peaks. Correlation time values in each class are presented in Table 2. The global coherence of the results is confirmed by the fact that correlation times between protons belonging to two different classes are on average shorter than the correlation times between protons of the two corresponding classes.

TABLE 2: Proton−Proton Correlation Times in 1a and 1b Given in Nanoseconds[a]

classes	**1a**	**1b**
T	0.64 ± 0.02 (18)	0.66 ± 0.07 (10)
B	0.69 ± 0.04 (9)	0.71 ± 0.11 (6)
C	0.54 ± 0.06 (20)	0.60 ± 0.04 (10)
M_{AD}	0.61 ± 0.03 (4)	0.59 ± 0.01 (2)
M_{BE}	0.45 ± 0.07 (3)	0.57 ± 0.01 (2)
M_{CF}	0.49 ± 0.02 (3)	

[a] Values with a relative error greater than 40% were discarded. Results are grouped according to the corresponding proton classes T, B, M, and C. (See the text and Figure 2.) The number of measured correlation times is given in parentheses. Only intraclass values are given.

A comparison of correlation times between classes was performed using Student tests at the 95% level of confidence. Significant differences are observed. We previously mentioned that under the conditions of xenon pressure used for the present study less than 0.3% of the cage should be empty. This dismisses the possibility that the mobility observed in the cryptophane cage comes from the time in which the cage is empty. It is observed on a time scale much shorter than the residence time of xenon inside the cage (around 0.75−0.85 ms under a pressure of 99 kPa). Thus, the scarce event of insertion or expulsion of a xenon atom from the cryptophane cavity cannot explain the observed difference in correlation times. Therefore, correlation times are indicative of cages filled with xenon. The significant differences between classes belonging to the same molecule show that cryptophane cages continue to be subjected to internal motions. This is in accordance with the above-mentioned simulation indicating that no significant decrease in cryptophane mobility in structures **1a** and **1b** is observed when inserting in silico a xenon atom into the cavity.

For both classes, no significant differences between classes T and B are observed. However, in **1a** but not in **1b**, the correlation time of class C is significantly shorter than that of class B. The higher mobility of class C in **1a** is interpreted as originating from the contribution of the pseudofree rotation of camphanate relative to cryptophane in the absence of van der Waals contacts between the cage and camphanate that could hinder free rotation.

The correlation times of M_{BE} are significantly shorter than in classes T and B in both cage molecules. Again, this is interpreted as a higher mobility of these elements: the CH_2-CH_2 groups are able to fluctuate relative to the neighboring atoms linked to the aromatic rings. M_{CF} has the same behavior at least in **1a** because no experimental value is obtained in **1b**.

In **1a**, M_{AD} correlation times are significantly longer than from those in the two other linkers, but this is not observed in **1b**. This observation could lead to the following interpretation. In **1a**, the mobility of the AD linker is lowered because of van der Waals interactions with the camphanate moiety. This also occurs in **1b**. However, because the cryptophane cavity of **1b** is elongated and not spherical as it is the case of **1a**, the xenon inside the cavity also limits the mobility of the M_{BE} linker. Thus, not only the entrance and exit of xenon are slowed (higher energy barriers for the binding) but also the respiration motions are slow and could be of higher amplitude because coalescence effects are visible in the ^{1}H NMR spectrum. Because of the capability of deformation of the cavity along an axis joining the two cyclotriveratrylene groups, xenon can find several locations inside it. Thus, a gain in entropy favors the binding relative to inclusion in **1a**.

Conclusions

This paper describes the solution behavior of two optically active cryptophane-A derivatives in tetrachloroethane in the presence of xenon. As evidenced in SPINOE experiments, these molecules strongly bind xenon by including it in the cryptophane cavity. The ^{129}Xe spectra at two pressures of the laser-polarized noble gas in a solution mixture of these host molecules display slow exchange conditions, as for the case of cryptophane-A. These cage molecules, apparently identical, exhibit different behaviors for the binding of the noble gas. Xenon has a higher affinity for the cage of anti (+)-cryptophane (−)-camphanate (**1b**) than for the cage of anti (−)-cryptophane (−)-camphanate (**1a**). Also, the energy barriers for the binding of xenon in these host molecules are quite different. Xenon access to the cavity of the cryptophane moiety is more hindered for **1b** than for **1a**.

An explanation of these net differences seems to arise from their capabilities to adapt their structures to the guest molecule. Because the sole difference between both molecules is the orientation of the camphanate part relative to the ethylenedioxy linkers, a detailed study of the structure and dynamics of these cage molecules has been performed and has revealed some interesting features.

Dealing with the ethylenedioxy linkers, **1a** seems to experience more local fluctuations on the nanosecond time scale than **1b**, as observed by the proton correlation times. **1b** is subjected to intermediate-to-slow motions, as indicated by the coalescence conditions observed in the ^{1}H NMR spectrum.

When **1b** binds xenon, the cage becomes oblate, the size of the cavity fitting the xenon diameter. Moreover, molecular modeling reveals that several locations for xenon inside the cavity are possible, contrary to the situation for **1a**, where the position of xenon seems to be fixed at the center of a spherical cavity.

All of these observations could lead to the following interpretation. The situation where the cage−camphanate relative rotation is hindered is energy stabilized in **1b** relative to that in **1a**. In the case of **1b**, van der Waals interactions between camphanate and cryptophane rigidify the molecule. Thus, not only the entrance and exit of xenon are slowed (higher energy barriers for the binding) but also the respiration motions are slower. Because of the capability of deformation of the cavity, xenon can find several locations inside it. Thus, a gain in entropy favors the binding. This effect has already been observed for the binding of xenon in hydrophobic pockets in proteins, where most of the time xenon is delocalized around several sites.[17−19]

These results give insight into the importance of the stereospecificity of the cryptophane derivatives for xenon binding. For the purpose of biosensing with xenon, the optimization of the vector molecule cannot circumvent an adequate choice not only of the nature of the substituent but also of the diastereomery of the compound.

Material and Methods

Chemicals. Rubidium 99.6% was purchased from Aldrich Chemical Inc. Xenon in natural isotopic proportions is from Air Liquide, and xenon enriched at 96% in isotope 129 is from Chemgas. Deuterated 1,1,2,2-tetrachloroethane (99.6%) is from Eurisotop.

Sample Preparation. 1a and **1b**, a mixture of both, and cryptophane-A samples[4] were prepared from powders and dissolved in deuterated tetrachloroethane to concentrations of 1.5 to 5 mM and were previously degassed by several freeze−pump−thaw cycles before introducing xenon gas either in natural isotopic abundance or, for SPINOE experiments, as ^{129}Xe enriched gas. Off-resonance ROESY experiments were performed with 1.6 mM samples.

For ^{129}Xe spectra and SPINOE experiments, xenon was polarized to ca. 15% via our homemade optical pumping apparatus.[15] Briefly, a tunable titanium:sapphire laser pumped by an argon ion laser produced a beam of ca. 5-W continuous power. This infrared light crossed a beam expander, a beam splitter cube, and finally a $\lambda/4$ plate. The beam, circularly polarized, then reached a cell of volume 100 cm^3 containing nitrogen, xenon, and a few milligrams of rubidium. The tunable laser was adjusted to the D1 electronic transition of the rubidium atoms. Heating the cell to ca. 363 K in the presence of a magnetic field of 56 G collinear to the light beam allowed optical pumping to occur. The so-called spin-exchange method[20] transfers light polarization to the electronic spins of the alkali metal and then, through collisions, to the nuclear spin of xenon. After a few minutes of optical pumping, xenon is separated from nitrogen by passing the gas mixture to a trap cooled by liquid nitrogen and surrounded by a solenoid producing a magnetic field of ca. 5 kG. Polarized xenon is then transferred, in the fringe field of the NMR magnet, to the NMR tube containing the solution of interest. After vigorous shaking for ca. 15 s and waiting about 30 s for temperature equilibration, NMR spectra were recorded.

NMR Experiments. The NMR experiments were performed at 11.7 and 14.0 T on Bruker DRX spectrometers equipped with 5-mm broadband inverse or direct probeheads. Signal integrations were performed using Peakfit software 4.11, distributed by SPSS Inc.

^{129}Xe chemical shifts are referenced to the peak of xenon free in solution, given at 229.5 ppm at 278 K^{-1}, and referenced to 228.0 ppm at 283 K through a series of xenon spectra of the sample of cryptophane-A, **1a**, and **1b** at various temperatures.

^{1}H chemical shifts are referenced to the d_2-tetrachloroethane chemical shift at 6.000 ppm at 281 K.

The assignment of ^{1}H and ^{13}C NMR spectra of **1a** and **1b** was performed at 274 K under a xenon pressure of ca. 170 kPa from a set of gHSQC, gHMBC, NOESY, off-resonance ROESY, and COSY spectra using SPARKY software.[21] For the cryptophane part, good resolution was necessary in both dimensions because of spectral overcrowding. The strategy consisted of assigning aromatic spin systems, composed of 2 ^{1}H and 6 ^{13}C nuclei, using gHSQC and gHMBC contour plots. For the latter, ^3J and ^2J ^{1}H−^{13}C couplings were observed, but ^3J couplings appeared to be significantly stronger than ^2J couplings, as observed and calculated at the INDO level of approximation on monosubstituted benzenes[22] and on π-benzenechromium tricarbonyl.[23] Then, methylenic spin systems, previously individualized by COSY and gHSQC spectra, were connected to aromatic rings on the molecule thanks to NOESY and gHMBC spectra. Stereospecific assignment of methylene protons was performed on the basis of NOE and off-resonance ROE signal intensities, more intense between aromatic and He protons than between aromatic and Ha protons. Methoxy protons were assigned thanks to correlations on gHMBC maps originating from ^3J ^{1}H−C−O−^{13}C couplings. The missing correlation obviously corresponded to the ring linked to the camphanate moiety, allowing the complete assignment on the corresponding cyclotriveratrylene. Ethylenedioxy protons (Hj and Hk), when possible, were assigned by following the same strategy as for the methoxy protons. Finally, NOESY correlations between Hj and Hk allowed the relative positioning of the two cyclotriveratrylene groups, achieving the almost complete proton assignment of the molecule. ^{1}H assignment at 281 K was performed by comparing off-resonance ROESY spectra at 274 and 281 K.

The off-resonance ROESY spectra were acquired at 281 K, with the angle θ between the spin-lock field axis and the static field axis taking values of 54.7, 40, 30, 20, and 0° (the last value being NOESY spectra) and mixing times of 50, 100, and 200 ms. The proton magnetization build-up curves were converted to effective cross-relaxation rates using the initial build-up rate approximation, and the evolution of these rates according to the angle θ gave access to the pure longitudinal and transverse cross-relaxation rates. Then, by assuming a single-exponential dipolar autocorrelation function for each proton pair, interproton distances and correlation times were extracted.[12]

Only correlation times determined with a relative precision better than 40% were retained. When two experimental values from the same pair of protons were derived from peaks symmetrical with respect to the diagonal in off-resonance ROESY spectra, both values were taken into account in the final averaging.

Computational Methods. The simulations have been performed using CNS1.1 software[24] under Linux Redhat 7.2. Because no topology or parameter files are available for these molecules, they have been built step by step. Some parameter values such as bond lengths and angles, partial charges, and nonbonded parameters have been adapted from Kirchhoff et al.[25,26] The generic topology file (for all cryptophane families) has been entirely built from zero. The second step was to create the molecular topology file specific for the molecule under study. Two identical cyclotriveratrylene fragments were assembled via a patch. The Cartesian coordinates of the camphanate moiety were taken from a pdb file of (−)camphor found on the web (http://xplor.csb.yale.edu/xplor-info/hetero/CAM-.html). The grafting of the camphanate part on one cyclotriveratrylene group was performed via another patch built from scratch.

The next step was to build a "generic" cryptophane molecule with reasonable covalent energies (what could also be called a prefolded structure). This step consisted of simulated annealing in order to avoid being blocked in local energy minima. To ensure that the molecule is roughly spherical, during this molecular dynamics, "anti-NOE" constraints, consisting of minimal distances between methylene bridges of opposite cyclotriveratrylene moieties, were introduced. They were removed just after this initial construction.

From each of these generic cryptophane molecules, a simulated annealing repeated 100 times with random initial atom velocities was run with the introduction of the proton−proton distance restraints. A first high-temperature Cartesian dynamics was performed for 30 ps at 50 000 K (time step 0.015 ps). In this step, the weight on the repulsive van der Waals term was divided by 10 to avoid hot energy spots in covering a large conformational space. Then, a slow cooling from 2000 to 0 K was performed (time step 0.005 ps, temperature step 25 K). During this step, the weight on the repulsive van der Waals term was progressively increased until its normal value and the shape of the NOE potential changed from asymptotic to quadratic form. Finally, the structures were optimized via 2000 steps of Powell minimization.

Acknowledgment. We thank the French Ministry of Research for financial support (ACI no. 4103 to H.D.).

References and Notes

(1) Bartik, K.; Luhmer, M.; Dutasta, J.-P.; Collet, A.; Reisse, J. *J. Am. Chem. Soc.* **1998**, *120*, 784.

(2) Souteyrand, E.; Nicolas, D.; Martin, J. R.; Chauvet, J. P.; Perez, H. *Sens. Actuators, B* **1996**, *33*, 182.

(3) Spence, M. M.; Rubin, S. M.; Dimitrov, I. E.; Ruiz, E. J.; Wemmer, D. E.; Pines, A.; Qin Yao, S.; Tian, F.; Schultz, P. G. *Proc. Natl. Acad. Sci. U.S.A.* **2001**, *98*, 10654.

(4) Brotin, T.; Barbe, R.; Darzac, M.; Dutasta, J.-P. *Chem.—Eur. J.* **2003**, *9*, 5784.

(5) Luhmer, M.; Goodson, B. M.; Song, Y.-Q.; Laws, D. D.; Kaiser, L.; Cyrier, M. C.; Pines, A. *J. Am. Chem. Soc.* **1999**, *121*, 3502.

(6) Brotin, T.; Devic, T.; Lesage, A.; Emsley, L.; Collet, A. *Chem.—Eur. J.* **2001**, *7*, 1561.

(7) Lowery, T. J.; Rubin, S. M.; Ruiz, E. J.; Spence, M. M.; Winssinger, N.; Schultz, P. G.; Pines, A.; Wemmer, D. E. *Magn. Reson. Imaging* **2003**, *21*, 1235.

(8) Sears, D. N.; Jameson, C. J. *J. Chem. Phys.* **2003**, *119*, 12231.

(9) Brotin, T.; Dutasta, J.-P. *Eur. J. Org. Chem.* **2003**, 973.

(10) Garel, L.; Dutasta, J.-P.; Collet, A. *Angew. Chem., Int. Ed. Engl.* **1993**, *32*, 1169.

(11) Segebarth, N.; Aitjeddig, L.; Locci, E.; Bartik, K.; Luhmer, M. *XEMAT*, International Symposium on Xenon NMR of Materials, La Colle sur Loup, Nice, France, May 29−31, 2003.

(12) (a) Berthault, P.; Birlirakis, N.; Rubinstenn, G.; Sinaÿ, P.; Desvaux, H. *J. Biomol. NMR* **1996**, *8*, 23. (b) Desvaux, H.; Berthault, P. *Prog. NMR Spectrosc.* **1999**, *35*, 295.

(13) Navon, G.; Song, Y.-Q.; Rõõm, T.; Appelt, S.; Taylor, R. E.; Pines, A. *Science* **1996**, *271*, 1848.

(14) Song, Y.-Q.; Goodson, B. M.; Taylor, R. E.; Laws, D. D.; Navon, G.; Pines, A. *Angew. Chem., Int. Ed. Engl.* **1997**, *36*, 2368.

(15) Desvaux, H.; Gautier, T.; Le Goff, G.; Pétro, M.; Berthault, P. *Eur. Phys. J. D* **2000**, *12*, 289.

(16) Desvaux, H.; Huber, J. G.; Brotin, T.; Dutasta, J.-P.; Berthault, P. *ChemPhysChem* **2003**, *4*, 384.

(17) Dubois, L.; Parrès, S.; Huber, J. G.; Berthault, P.; Desvaux, H. *J. Phys. Chem. B* **2004**, *108*, 767.

(18) Landon, C.; Berthault, P.; Vovelle, F.; Desvaux, H. *Protein Sci.* **2001**, *10*, 762.

(19) Dubois, L.; Berthault, P.; Huber, J. G.; Desvaux, H. *C. R. Physique* **2004**, *5*, 305.

(20) Walker, T. G.; Happer, W. *Rev. Mod. Phys.* **1997**, *69*, 629.

(21) Goddart, T.; Kneller, D. *SPARKY 3*; University of California: San Francisco, CA, 2004.
(22) Ernst, L.; Wray, V. *J. Magn. Reson.* **1977**, *25*, 123.
(23) Aydin, R.; Günther, H.; Runsik, J.; Schmickler, H.; Seel, H. *Org. Magn. Reson.* **1980**, *13*, 210.
(24) Brünger, A. T.; Adams, P. D.; Clore, G. M.; DeLano, W. L.; Gros, P.; Grosse-Kunstleve, R. W.; Jiang, J.-S.; Kuszewski, J.; Nilges, M.; Pannu, N. S.; Read, R. J.; Rice, L. M.; Simonson, T.; Warren, G. L. *Acta Crystallogr.* **1998**, *D54*, 905.
(25) Kirchhoff, P. D.; Bass, M. B.; Hanks, B. A.; Briggs, J. M.; Collet, A.; McCammon, J. A. *J. Am. Chem. Soc.* **1996**, *118*, 3237.
(26) Kirchhoff, P.; Dutasta, J.-P.; Collet, A.; McCammon, J. *J. Am. Chem. Soc.* **1999**, *121*, 381.